2

Liquid Crystals into Planar Photonic Crystals

Rolando Ferrini
Laboratoire d'Optoélectronique des Matériaux Moléculaires (LOMM),
Ecole Polytechnique Fédérale de Lausanne (EPFL)
Switzerland

1. Introduction

In the last decade, great effort has been devoted to the study of photonic crystals (PhCs), which are a new class of artificial materials that consist of a periodic arrangement of dielectric or metallic elements in one, two or three dimensions (see Figs. 1-2). The periodicity of these dielectric structures affects the properties of photons in the same way as the periodic potential affects the properties of electrons in semiconductor crystals. Consequently, light propagation along particular directions is forbidden within large energy bands known as photonic bandgaps. Due to such unique properties, PhCs have been proposed as a promising platform for the fabrication of miniaturized optical devices whose potential has been demonstrated both theoretically and experimentally in several applied and fundamental fields such as integrated optics and quantum optics (Busch et al., 2004; Lourtioz et al., 2005).

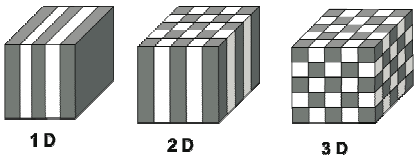

Fig. 1. Sketch of one- (1D), two- (2D) and three-dimensional (3D) photonic crystals (Joannopolous et al., 2008).

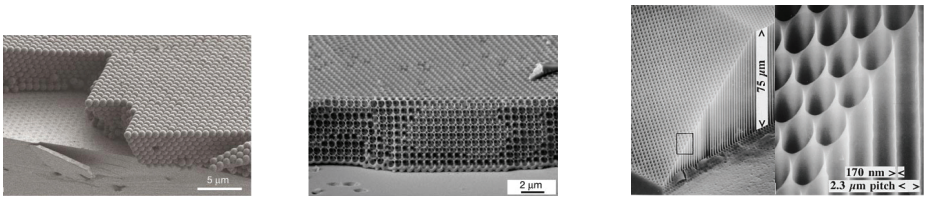

(a) (b) (c)

Fig. 2. Scanning electron microscopy images of three- [(a) opal and (b) inverse opal layers] and two-dimensional [(c) patterned and micromachined layer of macroporous silicon] photonic crystals [(a)-(b) Vlasov et al., 2001; (c) Grüning et al., 1995].

In particular, planar PhCs consisting of a periodic lattice of air holes etched through a high refractive index dielectric matrix (in general, a semiconductor-based vertical step-index

waveguide providing the vertical light confinement: see Fig. 3) have been intensively studied as artificial materials that offer the possibility to control light propagation on the wavelength scale. For instance, PhC-based optical cavities with high quality factors have been proposed for the demonstration of cavity quantum electro-dynamic effects such as the control of spontaneous emission or the fabrication of single photon sources. Moreover, PhC devices have been studied as building blocks in wavelength division multiplexing applications for integrated optics, where the information is coded into light signals that are treated by either active or passive PhC components such as lasers, filters, waveguides, bends and multiplexers.

(a) (b)

Fig. 3. Scanning electron microscopy images of (a) InP-based substrate-like and (b) GaAs-based membrane-like planar photonic crystals [(a) Ferrini et al., 2002a; (b) Sugimoto et al., 2004].

Nowadays, due to this extensive research effort, the conception and fabrication of such photonic structures have gained a complete maturity leading to the realization of the first real applications. PhC devices are routinely fabricated and their optical properties may be optimized at the design stage by modifying the size and/or the position of the air holes either inside or at the boundaries of the device (Song et al., 2005). Nevertheless, PhC-based structures are often lacking in versatility and tunability: On one hand, there are still a few factors that limit the use of PhCs in real devices, such as fabrication imperfections, losses and temperature sensitivity (Ferrini et al., 2003a-b; Wild et al., 2004). On the other hand, as a fundamental requirement for any practical application, the possibility should be guaranteed to adjust the optical properties of the fabricated components by external means. Therefore, the research has focused on the possibility of increasing the device functionalities either by correcting (after fabrication: trimming) or by controlling (on demand: tuning) the optical properties of the PhC in order *i*) to compensate either the temperature sensitivity or the imperfections of the PhC itself (Wild et al., 2004), *ii*) to create reconfigurable devices for integrated optics (Busch et al., 2004; Lourtioz et al., 2005), *iii*) to fabricate bio-chemical sensors (Barthelemy et al., 2007), and *iv*) to conceive new optical functions (Mingaleev et al., 2004). It is worth highlighting that this innovative and emerging research domain may have a huge potential for technological breakthroughs in various application fields such as integrated optics, quantum optics, detection and sensing.

The optical properties of PhCs can be modified by changing the optical length of the PhC structure. This can be achieved either by adjusting the geometrical parameters that define the PhC lattice, *e.g.* the lattice period (*i.e.* the filling factor f) (Joannopolous et al., 2008), or by modifying the refractive indexes of the PhC components. In the first case a mechanical stress may be applied to the PhC slab (Wong et al., 2004), whilst, in the second approach, it is possible to act either on the high index or on the low index component.

As for the high index (*e.g.* the semiconductor) medium, the standard tuning techniques used in classical optoelectronic devices can be applied to modify its refractive index by temperature, by optical pumping or by applying an external magnetic or electric field. For instance, in InP-, GaAs-, or Si-based PhCs, since the semiconductor thermo-optical coefficients are in the order of several 10^{-4}/°C, the thermo-optical effect has been largely used to modulate the optical response (Takeda & Yoshino, 2003; Wild et al., 2004; Tinker & Lee, 2005). Moreover, fast modulation rates in the order of ps down to fs have been obtained by both resonant (*i.e.* by means of carrier injection) and non-resonant (*i.e.* by exploiting the Kerr effect) optical pumping (Haché & Bourgeois, 2000; Leonard et al., 2002; Baba et al., 2003; Ndi et al., 2005; Raineri et al., 2005; Britsow at al., 2006; Hu et al., 2006; Ndi et al., 2006; Teo et al., 2006; Hu et al., 2007; Tanabe et al., 2007).
When either magnetic or ferro-electric or electro-optic non-linear materials are used to fabricate PhC devices, external magnetic or electric fields can be applied, respectively, to adjust the optical response (Kee et al., 2000; Lyubchanskii et al., 2003; Scrymgeour et al., 2003; Belotelov & Zvezdin, 2005).
Finally, other external means like mechanical probes or micro-electromechanical actuators (Märki et al., 2006; Kanamori et al., 2007) have been explored to tune the optical properties of the high index matrix and thus the PhC optical performances.
In the case of semiconductor-based planar PhCs, the classical tuning techniques described above are not always suitable for all the envisaged optics and photonics applications. For example, although the potential of temperature tuning, carrier injection and optical pumping has been fully demonstrated even in real devices, they still present a few intrinsic limits. On one hand, in planar PhC circuits, the large thermal conductivity of the semiconductor matrix makes difficult the temperature tuning of a single device on a chip (Wild et al., 2004). On the other hand, the optical pumping methods require high power optical sources that cannot always be easily integrated in an optical circuit (Teo et al., 2006) and can often change only locally the PhC response.
Therefore, in the last few years, the PhC community has considered with greater and greater attention the alternative approach consisting in the replacement of the low index component (*i.e.* the air) with a different material that can offer further degrees of tunability. Namely, if the refractive index of the infiltrated material can be modified by an external factor (*e.g.* electrical or magnetic fields, light irradiation, temperature, etc.), one can easily adjust and modulate the optical properties of the infiltrated PhC, thus enabling the development of tunable PhC devices for different application fields. Among the numerous techniques that have been proposed, infiltrating the air pores of a PhC with a synthetic organic material that has a tunable refractive index (*e.g.* liquid crystals, polymers, liquids, and liquid dispersions of colloidal quantum dots) has proved to be one of the most promising approaches for both trimming and tuning (Busch & John, 1999; Yoshino et al., 1999b; Leonard et al., 2000; Kubo et al., 2002; Gottardo et al., 2003; Mertens et al., 2003; Schuller et al., 2003; Maune et al., 2004; Mingaleev et al., 2004; Weiss et al., 2005a; Erickson et al., 2006; Ferrini et al., 2006; Haurylau et al., 2006a-b; Intonti et al., 2006; Martz et al., 2006; Tomljenovic-Hanic et al., 2006; van der Heijden et al., 2006a; Barthelemy et al., 2007; Smith et al., 2007; Tay et al., 2007). The effect of infiltrating a PhC with a low refractive index material is qualitatively shown in Fig. 4, where the transmission through a ΓM-oriented triangular lattice of holes (see Sect. 2.1, Fig. 5) etched in a dielectric matrix is simulated for the transverse electric (TE) polarization and for different refractive index values inside the holes. Once the PhC is infiltrated, due to the reduced refractive index contrast between the dielectric matrix and the holes, the photonic

bandgap shrinks and the band edges red-shift. In particular, since for energies located in the low- (dielectric) and high-energy (air) transmission bands the electric field of the propagating Bloch modes is concentrated in the dielectric and in the holes, respectively (Busch et al., 2004; Lourtioz et al., 2005; Joannopolous et al., 2008), the energy shift of the air band edge is one order of magnitude larger than the corresponding shift of the dielectric band edge.

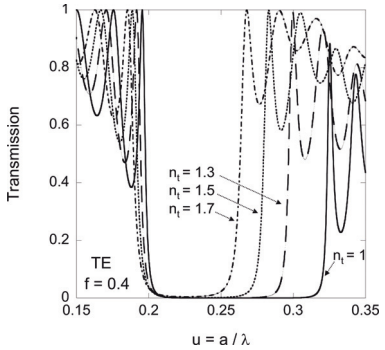

Fig. 4. Simulated transmission spectra through a ΓM-oriented triangular lattice of holes (air filling factor f = 0.4) etched in a dielectric matrix (n = 3.3) for the transverse electric (TE) polarization (see Fig. 5) and for different refractive indexes inside the holes: *i.e.* n_t = 1 (empty holes), 1.3, 1.5, and 1.7 (El-Kallassi, 2009).

The choice of organic molecules to fill the air holes of planar PhCs stems naturally from the following properties of organic materials:

- they offer a large variety of interesting optical properties both in the visible and in the near infrared spectral regions that often depend on the molecular organization;
- there exist a wide palette of different molecular organizations depending on the molecule interactions. The complex thermodynamic properties of such molecular mixtures enable one to easily modify the molecular order (*e.g.* by changing the temperature, by applying an electric field, by irradiating at certain wavelengths, etc.) and, thus, the optical properties of the material itself;
- the complex interaction between organic molecules and inorganic surfaces, such as the semiconductor native oxide layers, strongly affects the wetting properties of the organic blends. Therefore, controlling the surface quality allows one to control the molecule organization and the optical properties of the material itself.

Therefore, research efforts have been focused on the functionalization of PhC devices by trimming/tuning the optical properties of these organic materials. In particular, the potential of PhC infiltration with nematic liquid crystals (LCs) has been largely demonstrated for one-, two- and three-dimensional (1D, 2D and 3D) PhCs. Therefore, besides their classical fields of application, LCs are also having a strong impact in the PhC field (Busch & John, 1999; Yoshino et al., 1999b; Leonard et al., 2000; Kang et al., 2001; Shimoda et al., 2001; Kubo et al., 2002; Mertens et al., 2002; Gottardo et al., 2003; Mertens et al., 2003; Schuller et al., 2003; Weiss & Fauchet, 2003; Busch et al., 2004; Du et al., 2004; Kubo et al., 2004; Martz et al., 2004; Maune et al., 2004; Kosmidou et al., 2005; Lourtioz et al., 2005; Maune et al., 2005; Weiss et al., 2005a-b; Ferrini et al., 2006; Haurylau et al., 2006b; Martz et al., 2006).

The molecule shape and their long-range orientational order are at the origin of the optical anisotropy of a nematic LC, which is a birefringent medium with an uniaxial symmetry. When interacting with the nematic LC, light experiences the ordinary refractive index (n_o) or the extraordinary refractive index (n_e) if the electric field is polarized perpendicularly or parallel to the axis of the LC molecules, respectively. The molecular order of a LC can be easily modulated by means of external perturbations, thus allowing one to adjust their dielectric constant (*i.e.* the refractive index) on demand. Consequently, the optical response of a PhC infiltrated with nematic LCs can be either trimmed or tuned by applying an external electric field which modifies the orientation of the molecules with respect to the polarization direction of a light beam propagating through it. Moreover, when the temperature is increased above the nematic-isotropic phase transition temperature (clearing point), the molecular order is destroyed and the LC is in its isotropic phase: its optical properties are thus characterized by an isotropic refractive index (n_i) that is independent of the molecule orientation. Finally, when nematic LCs are mixed with photosensitive molecules like photochromes (see below), the latter phase transition can be photoinduced isothermally by light irradiation at certain wavelengths. All these tuning mechanisms are reversible and they have been exploited to tune the optical properties of PhC structures infiltrated with nematic LCs (Alagappan et al., 2006; Halevi et al., 2006; Haurylau et al., 2006a-b; Martz et al., 2006; Anderson et al., 2007; Reyes et al., 2008).

In this chapter, we will show how the infiltration of LCs in the air holes of III-V semiconductor-based planar PhCs can be used to both trim and tune the optical properties of PhC devices by controlling the orientation of the LCs inside the nanometer-size holes by means of a temperature, electrical or optical trigger.

In Section 2, we will illustrate the main optical properties of the InP-based substrate-like planar PhCs consisting of a hexagonal array of air holes (hole diameter = 200 – 400 nm; air filling factor f = 0.40-0.50) that were mainly used for our studies. Moreover, the choice of the nematic LCs [*i.e.* LC-K15 (5CB)] will be briefly discussed and their optical properties will be summarized (Martz et al., 2004; Martz et al., 2005).

In Section 3, we will focus on the infiltration of LC molecules in cylindrical holes with a diameter of a few 100's nm by means of a vacuum chamber specifically designed to empty the gaseous content of the holes, to clean and, when necessary, to chemically activate the device surface (Martz et al., 2004; Martz et al., 2006). The reliability and reproducibility of the infiltration process are assessed by the optical characterization of the infiltrated structures. Moreover, we note that, in order to exploit the tunable optical properties of nematic LCs for the functionalization of PhC devices, it is important to know both the filling efficiency and the orientation of the molecules inside holes. This latter property eventually depends both on the physics of the infiltration process of an organic viscous liquid in nanometer-size holes and on the surface aligning properties of the structured semiconductor matrix. In the last two decades, the LC community has made great efforts to understand the organization of LC molecules confined in nanometer-size cylinders. Both theoretical and experimental studies have been performed to quantify the influence of the surface anchoring and of the hole size on the LC molecular organization (Crawford et al., 1991a-b; Marroum et al., 1995; Burylov, 1997). With regard to this issue, we will show how optical measurements as a function of temperature and polarization can yield information on both the hole filling and the molecule orientation (Martz et al., 2006; Ferrini et al., 2006).

In Section 4, we will show how the optical response of PhC devices infiltrated with nematic LCs can be tuned by temperature, electric field and optical irradiation (Ferrini et al., 2006;

El-Kallassi et al., 2007). In particular, we observe that, in spite of a large amount of research on LC infiltrated PhCs, little has been done on their optical tuning (Maune et al., 2005), even though all-optical switching plays a very important role in the optical communication field (Asakawa et al., 2006) and, as we have briefly discussed above, several other approaches have already been explored to optically tune planar PhCs (Ndi et al., 2005; Raineri et al., 2005; Teo et al., 2006; Tanabe et al., 2007). Here, we will illustrate how it is possible to optically tune the response of planar PhC devices by infiltration with a photo-responsive LC blend doped with azobenzene photochromic molecules (Legge & Mitchell, 1992; Sung et al., 2002; Ikeda, 2003).

2. Photonic crystals and liquid crystals

2.1 InP-based planar photonic crystals

Planar PhCs consisting of a triangular lattice of air holes were etched by chemically assisted ion beam etching (CAIBE) through a nominally undoped InP/(Ga,In)(As,P)/InP vertical waveguide grown by metalorganic vapour phase epitaxy on a (100) *n*-doped InP substrate: see Fig. 4a (Ferrini et al., 2002b; Ferrini et al.; 2004; Mulot et al., 2004). In the wavelength range of interest (*i.e.* $\lambda \approx 1.5$ μm) the waveguide is single-mode for both the transverse electric (TE) and magnetic (TM) polarization directions (*i.e.* electric field perpendicular and parallel to the hole axis, respectively: see Fig. 5a) and the effective refractive indexes n_{eff} for both the TE and the TM guided modes varies linearly with temperature (Wild et al., 2004; Ferrini et al., 2004; Mulot et al., 2004; Martz et al., 2005; Ferrini et al., 2006; El-Kallassi et al., 2007).

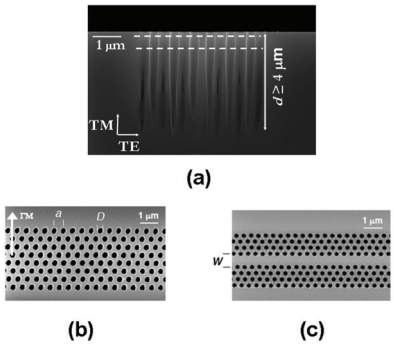

Fig. 5. Scanning electron microscopy images (El-Kallassi et al., 2007): (a) Cut view of a PhC etched through a InP/(Ga,In)(As,P)/InP planar waveguide [the GaInAsP core layer is sketched (dashed lines)]: the hole depth is d ≥ 4 μm. The white arrows indicate the orientation of the electric field for the transverse electric (TE) and magnetic (TM) polarization directions; (b) Top view of a 8-rows thick ΓM-oriented PhC slab (*a* = lattice period; D = hole diameter); (c) Top view of a Fabry-Perot cavity between two 4-rows thick ΓM –oriented PhC mirrors (*W* = cavity width).

A scanning electron microscopy cut view of the obtained PhCs appears in Fig. 4a: the hole depth *d* is of the order of 4 μm. Two types of structures were fabricated (see Figs. 5b-c): *i*) 8 rows-thick ΓM-oriented PhC slabs; and *ii*) Fabry-Pérot (FP) cavities consisting of two 4-rows thick ΓM-oriented PhC mirrors separated by a spacer *W*.

The internal light source (ILS) technique was used to optically characterize the infiltrated PhC structures (Ferrini et al., 2002b). To this aim, two GaAsInP quantum wells (QWs) were embedded in the core layer to act as a built-in light probe for optical measurements. The superimposition of the two QW emission peaks yields a 100 nm-wide photoluminescence (PL) spectrum centered at λ = 1.5 μm. The PL excited inside the QWs is used as a built-in probe beam. Part of the PL signal propagates parallel to the surface as a guided mode and interacts with the PhC structure before escaping from a cleaved edge and being collected and spectrally analyzed. The absolute PhC transmission is obtained normalizing the spectrum measured after transmission through the PhC slab with respect to a spectrum collected in a non-patterned region of the sample. Since ILS measurements on a single PhC structure yield the transmission spectrum only in a narrow spectral interval (~ 100 nm), the PhCs were replicated with different periods a (*i.e.* a = 300-600 nm with Δa = 20 nm) while keeping constant the intended air filling factor f = 0.40-0.50 (lithographic tuning). Thus, due to the scaling property of PhCs (Joannopolous et al., 2008), the absolute transmission through the PhC structures was measured as a function of the normalized photon energy $u = a/\lambda$ (energy reduced units). The real filling factor f was then measured by fitting the transmission spectra of the empty structures (Ferrini et al., 2002b). We obtained an average value $f = 0.43 \pm 0.01$ that corresponds to a hole diameter D = 200 – 400 nm.

2.2 Nematic liquid crystals

Commercial nematic LCs by Merck® were used to infiltrate the fabricated PhC structures. While preliminary experiments were performed with LC-E7, a blend of a cyanoterphenyl and several cyanobiphenyl molecules (see Fig. 6a), for the infiltration of the InP-based planar PhCs we chose LC-K15 that consists of only one type of molecules [4-cyano-4'-pentylbiphenyl (5CB): see Fig. 6b]. This latter property guarantees the stability of LC-K15 with respect to the infiltration procedure, during which the LC blend is heated at low pressure (see Sect. 3). This was verified by means of differential scanning calorimetry measurements, where the LC response was analysed before and after heating the molecule blends at low pressure, *i.e.* in similar conditions as during the in-filling process. While a change in the blend composition was detected in the LC-E7 blend, for the LC-K15 molecules the location of the peaks in the heat capacity signals (see Fig. 7a), which correspond to the nematic-to-isotropic phase transition (Mansare et al., 2002), does not change after the treatment, thus showing that the physical-chemical properties of LC-K15, as well as its optical properties (*i.e.* the refractive index), remain stable after the infiltration.

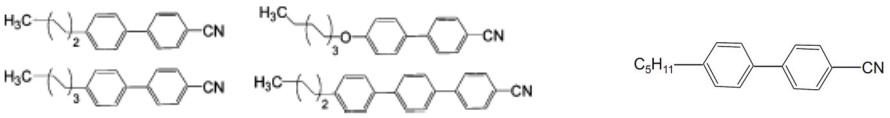

LC-E7 (a) **LC-K15 (5CB)** (b)

Fig. 6. Chemical structure of the used nematic liquid crystals (by Merck®): (a) LC-E7 blend [one cyanoterphenyl and three cyanobiphenyl molecules] and (b) LC-K15 [4-cyano-4'-pentylbiphenyl (5CB)]. All molecules present an aromatic structure with polar cyano headgroups and apolar aliphatic tails [(a) Martz et al., 2004; (b) El-Kallassi et al., 2007].

In addition, LC-K15 has lower nematic-to-isotropic and nematic-to-polycrystalline phase transition temperatures than LC-E7: *i.e.* $T_{c1} = T_{NI}$(LC-K15) = 35 °C (clearing point) (see also Fig. 7a) and $T_{c2} = T_{KN}$(LC-K15) = 23 °C (melting point), respectively (Mansare et al., 2002). This makes LC-K15 more suitable than LC-E7 for infiltration and temperature tuning experiments (see Sect. 4).
Finally, in Fig. 7b, the ordinary n_o, extraordinary n_e, and isotropic n_i refractive index values of LC-K15 are reported as a function of temperature for a wavelength λ = 1.5 μm (Li & Wu, 2004). In particular, at T = 24 °C, n_o = 1.501 and n_e = 1.656, while, at T = 37 °C, n_i = 1.548 (Brugioni et al., 2006).

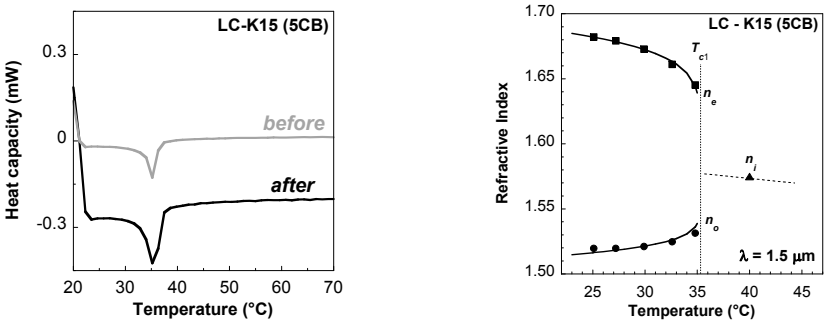

Fig. 7. Nematic liquid crystals LC-K15 (by Merck®): (a) Differential scanning calorimetry measurements on LC-K15 before (grey line) and after (black line) heating the LC at low pressure, *i.e.* in similar conditions as during the PhC infiltration process. (b) Ordinary n_o, extraordinary n_e, and isotropic n_i refractive index values of LC-K15 as a function of temperature. The nematic-to-isotropic phase transition temperature [$T_{c1} = T_{NI}$ = 35 °C (clearing point)] is reported. [(a) Martz et al., 2005; (b) Mansare et al., 2002; Li & Wu, 2004].

3. Infiltration of nematic liquid crystals in planar photonic crystals

3.1 Infiltration experiments

Using nematic LCs to fill InP-based planar PhCs, *i.e.* cylindro-conical holes with a diameter ranging from 200 up to 400 nm, an average depth of 4 μm and a closed bottom (see Fig. 5) is indeed far from being a trivial problem. For instance, when infiltrating nanoporous materials (*e.g.* nanometer-size tubes) with viscous liquids, the gravitational forces are several orders of magnitude smaller than the capillary forces, which eventually drive the infiltration process (Busch et al., 2004). The latter forces are proportional to the capillary diameter, the surface tension and the contact angle of the liquid on the tube surface (van der Heijden et al., 2006a-b). In particular, if this angle is lower than 90°, the capillary forces assist the infiltration, otherwise, for angles larger than 90°, the liquid is expelled from the tube. Therefore, in order to achieve a good infiltration efficiency (see Sect. 3.2), it is important to guarantee a LC wettability on the capillary surface as large as possible, *i.e.* the smallest possible contact angle. The liquid wettability on a solid surface depends on the chemical composition, the geometry and an eventual functionalization of the surface (Martz et al., 2004). In the case of III-V semiconductor-based (*e.g.* InP- or GaAs-based) planar PhCs, the sample surface tends to be hydrophobic, *i.e.* with a water contact angle larger than 90° (see

Fig. 8a). Nevertheless, chemical and/or plasma treatments, as well as chemical surfactants, can be used to increase the surface energy and thus to improve the wettability of such materials (D. Myers, 1991). For example, in Fig. 8a-b, the contact angle images of a water droplet on the surface of a non-patterned region of an InP-based PhC before and after a chemical attack with hydrofluoric (HF) acid are shown, respectively. The HF treatment removes the residual SiO_2 over-layer that is usually deposited on the InP surface for the fabrication of planar PhCs (Mulot et al., 2004) and contributes to strongly increase the water wettability on the sample, thus yielding a hydrophilic surface. In particular, LC contact angle images taken on the same surfaces show that, if LC-K15 presents already a good wettability (see Fig. 8c), the HF treatment yields a contact angle close to 0°, *i.e.* an almost perfect wettability.

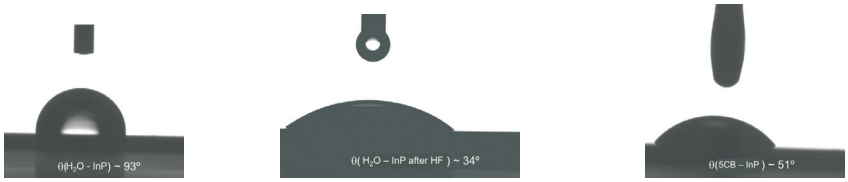

(a) (b) (c)

Fig. 8. Contact angle images of (a)-(b) water and (c) LC-K15 (5CB) liquid crystal droplets on the surface of a non-patterned region of an InP-based planar photonic crystal before and after a chemical treatment with hydrofluoric (HF) acid, respectively. For the LC-K15 (5CB) droplet, the HF treatment yields a contact angle close to 0°, *i.e.* an almost perfect wettability, so that no droplets can form on the surface (El-Kallassi, 2009).

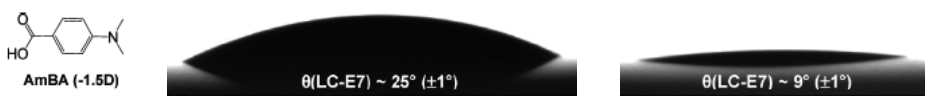

(a) (b) (c)

Fig. 9. Deposition of self-assembled monolayers of (a) a *p*-(dimethylamino)-benzoic acid (AmBA) on a doped GaAs surface: contact angle images of LC-E7 liquid crystal droplets on (b) an unmodified and (c) a functionalized surface. (Martz et al., 2004)

Moreover, if necessary, it is possible to functionalize the semiconductor surface with molecular self-assembled monolayers (SAMs), which have been demonstrated to be very important for the surface modification of several optoelectronics devices and are widely used as molecular orientation layers for LCs (Martz et al., 2004 and references therein). In particular, we demonstrated the possibility of using surface-adsorbed monolayers on oxidized GaAs surfaces to improve the LC wettability. The surface of GaAs is unstable in an atmosphere containing oxygen and water: after exposure to air, a native oxide layer is usually formed. This latter layer can be used as a binding layer for the deposition of carboxylated derivatives using a vapor growth method under high vacuum on doped plasma-activated GaAs surfaces. Due to the amphiphilic nature of LCs, as orientation layers, we chose para-substituted benzoic acids that exploit the affinity to the highly polar cyano headgroups and to the aromatic structure of LC-E7 (see Fig. 6a). In Figs. 9b-c, the contact angle images of LC-E7 droplets on an unmodified GaAs wafer and on a GaAs surface functionalized with a *p*-(dimethylamino)-benzoic acid (AmBA: see Fig. 9a) are shown,

respectively. This surface treatment strongly increases the LC-E7 wettability on the GaAs surface and static contact angles as small as 9° could be achieved.
In addition to the LC wettability, other parameters must be taken into account when infiltrating planar PhCs. If, in the case of 3D or 2D membrane-like PhCs, the samples can be partially immersed in a LC bath and, while LC molecules penetrate into the nanopores, the air is naturally evacuated, in substrate-based planar PhCs the air holes are accessible only from the top and the gas evacuation may be difficult. Indeed, it has been demonstrated both theoretically and experimentally that a low ambient pressure is beneficial to the infiltration process since it minimizes the effects of gas trapping in the LCs and contributes to drastically reduce the air volume that remains eventually encapsulated at the hole bottom (Leonard et al., 2000; Schuller et al., 2003; van der Heijden et al., 2006a-b). The residual air content is finally degassed through the LC column (Nielsen et al., 2005; van der Heijden et al., 2006a-b). Infiltration times of several minutes up to few hours were adopted in order to guarantee a complete gas evacuation and thus a perfect hole infiltration.
A vacuum chamber with controllable temperature and pressure was specifically designed for planar PhC infiltration experiments (see Fig. 10). The chamber is equipped with three sample holders and a small crucible containing the LCs that are heated by means of three resistances and a convection-heating ring, respectively; several thermocouples connected to the holders and to the crucible enable the separate control of the LC and the sample temperature. A pumping system allows the chamber pressure to be reduced down to 10^{-6} mbar and a vacuum gauge is used to control the vacuum level. A gas inlet (*i.e.* argon or nitrogen) is utilized to eventually release the chamber to the atmospheric pressure.

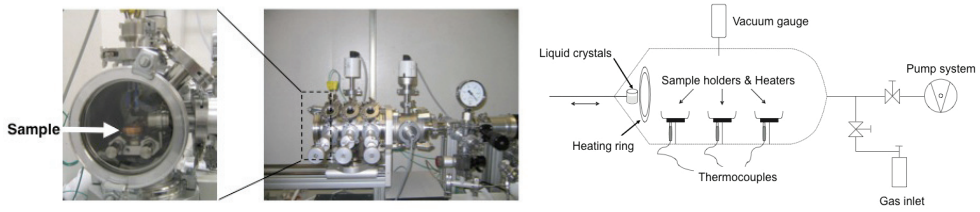

Fig. 10. (a) Images and (b) sketch of the vacuum chamber designed for the infiltration of planar photonic crystals (El-Kallassi, 2009).

The best temperature and pressure conditions were investigated to optimize the infiltration process and to improve its reliability and reproducibility. The chamber pressure is reduced to 10^{-5} mbar, which is enough to guarantee a small residual air content at the hole bottom (see above). The temperature is also a fundamental parameter: during the infiltration procedure, both the LCs and the samples are constantly kept at a temperature higher than the clearing point (*i.e.* 40 °C). This reduces the LC viscosity, thus favouring the pore infiltration, and avoids wall contamination by water residuals. The filling process itself can be divided into three steps: (*i*) *Evacuation*: The vacuum chamber is pumped to empty the gaseous content of the holes and to degas the LCs inside the crucible, which, to this aim, are heated at 30°C. This is indeed an essential step: if LCs are not properly degassed, trapped gases may combine to generate bubbles inside the holes, thus limiting the infiltration efficiency. (*ii*) *Contact*: The LCs are left in contact with the samples for several minutes up to few hours (see above). (*iii*) *Infiltration*: Finally, the vacuum chamber is instantaneously

brought to the atmospheric pressure and the sample is slowly cooled down to the ambient temperature. This is an important step for the infiltration process: the pressure differential between the chamber and the holes introduces a supplementary force that assists the hole filling.

A systematic characterization of the infiltration procedure was carried out by means of optical measurements. Several infiltration experiments were performed on the same PhC samples under the same temperature and pressure conditions. Before each infiltration the samples were heated at a temperature much higher than the clearing point (see Sect. 2.2) to evaporate the LC molecules, *i.e.* to empty completely the holes. In order to exclude the presence of LC residuals in the holes, after heating, the samples were cooled down to room temperature, where transmission spectra through the emptied PhC structures were measured and compared with the reference spectra taken before infiltration. The same results were found in terms of the optical properties of the PhCs after infiltration, thus testifying to the great reproducibility and reliability of the in-filling technique (J. Martz et al., 2005).

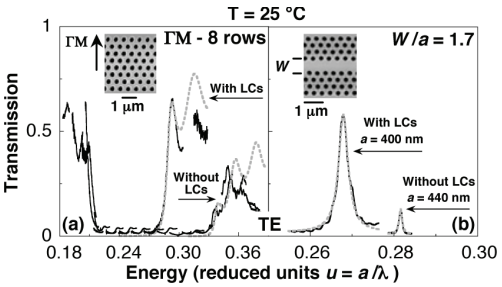

Fig. 11. Measured TE transmission spectra through (a) 8-rows thick ΓM-oriented PhC slabs (see the inset) and (b) a Fabry-Pérot (FP) cavity between two 4-rows thick ΓM-oriented PhC mirrors (see the inset) with and without LCs (black lines). *W* is the cavity width and *a* the PhC lattice period. The best-fit curves of the experimental spectra are shown (grey dotted lines) (Martz et al., 2006).

The TE polarized transmission spectra at room temperature through ΓM-oriented PhC slabs (see Fig. 5) without and with LCs are shown in Fig. 11a (black lines). A well-defined stopgap appears in the empty sample. Once the PhC is infiltrated, the photonic bandgap shrinks and the band edges red-shift (see Sect. 1). Moreover, the air band transmission increases, thus indicating a strong reduction of the PhC losses after infiltration. In low refractive index contrast planar PhCs perforating the vertical waveguide induces coupling of the guided wave to radiation modes into the claddings, thus resulting in out-of-plane losses (Ferrini et al., 2003a-b). When infiltrating PhCs with a material whose refractive index is higher than that of the air, the out-of-plane diffraction at the waveguide-hole interface is reduced. In order to confirm this, the spectra were fitted by means of a two-dimensional finite difference time domain (2D-FDTD) model assuming n_{eff} as the matrix index and n_{hole} as the hole refractive index (Qiu et al., 2002). Out-of-plane losses were included into the 2D model by adding a phenomenological imaginary dielectric constant ε″ in the holes (Ferrini et al., 2003a-b). The measured values $f = 0.42$ and 0.46 were assumed that correspond to the energy u (*i.e.* to the PhC period a in the lithographic tuning approach: see Sect. 2.1) where the fitted band edges are located in the spectra without and with LCs, respectively. The independent

fit parameters were ε″ and n_{hole}: the calculated spectra are shown in Fig. 11a (grey dotted lines). The values n_{hole} = 1 and 1.59, and ε″ = 0.045 and 0.030 were found for the PhCs without and with LCs, respectively, thus confirming the increase of n_{hole} and the consequent decrease of losses after infiltration.
Transmission spectra at room temperature through the FP cavities (see Fig. 5) without and with LCs are shown in Fig. 11b. Due to the increase of n_{hole}, the FP resonance red-shifts with respect to the empty sample. The FP peaks were fitted using an Airy's formula (Ferrini et al., 2002b): the calculated curves are shown in Fig. 11b (grey dotted lines). Due to the reduced refractive index contrast, after infiltration the mirror transmission increases from 0.013 to 0.090 while its reflectivity decreases from 0.96 to 0.887. Therefore, in agreement with the results obtained for simple slabs, the loss coefficient L = 1 - R - T decreases from 0.017 to 0.013. Due to the change of both the mirror optical properties and the cavity losses (Mulot et al., 2004; Martz et al., 2005), the peak transmission increases and the cavity quality factor decreases from 310 to 100.

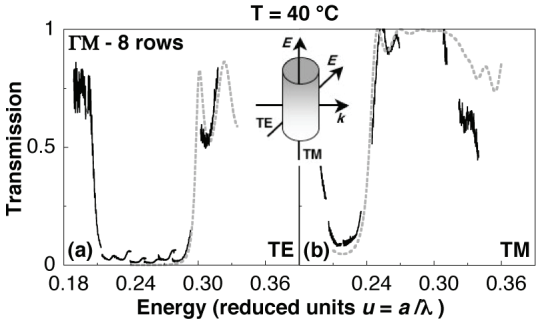

Fig. 12. Experimental (black lines) and calculated (grey dotted lines) (a) TE and (b) TM transmission spectra through infiltrated 8-rows thick ΓM-oriented PhC slabs (see Fig. 11) at T = 40 °C. The orientation of the E-field with respect to the hole axis and the light propagation direction (vector k) are sketched in the inset for both the TE and TM polarizations. (Martz et al., 2006).

3.2 Infiltration efficiency

The infiltration efficiency of substrate-like planar PhCs is a critical parameter, whose measurement is not easy (Schuller et al., 2003). While using standard scanning electron or atomic force microscopy is not straightforward, optical measurements have proved to be very useful in the characterization of infiltrated planar PhCs (Martz et al., 2005; Martz et al., 2006). The average infiltration efficiency η can be accurately determined by measuring the TE and TM transmission spectra (see black lines in Figs. 12a-b, respectively) through infiltrated PhC slabs at a temperature T = 40 °C > T_{c1}. Due to the birefringence of nematic LCs, the component of their dielectric constant along the electric field (and thus the effective LC refractive index n_{LC}) depends on the molecule orientation. However, when working at a temperature above the clearing point, LCs are in an isotropic phase and the dielectric constant is a scalar, independent from the molecule orientation and the field distribution, *i.e.* $n_{LC} = n_i$. As in Sect. 3.1, the TE and TM air band transmission edges were fitted by means of a 2D-FDTD model with f = 0.46 and 0.48, respectively, and ε″ and n_{hole} as free fitting parameters: the calculated spectra are shown in Fig. 12 (grey dotted lines). The fit yielded

the value n_{hole} = 1.50 for both polarizations, thus confirming that at T = 40 °C the infiltrated LCs are in their isotropic phase. The same result is obtained by the 2D-FDTD fit of the resonance energy in the transmission spectrum through the FP cavities. The infiltration efficiency is defined as the percentage of the PhC slab that is filled, *i.e.* $\eta = (n_{hole} - 1) / (n_{LC} - 1)$. Since $n_{LC} = n_i = 1.575$ (see Fig. 7 in Sect. 2.2), the value $\eta = 0.87$ is obtained. We remark that, whilst the same value is obtained for several hole diameters, η does not contain any local information on the partial or complete filling of individual holes.

3.3 Optical characterization of the molecule orientation

Once the infiltration efficiency is known, in order to identify the better mechanisms to tune the optical properties of the infiltrated PhCs, it is important to understand how the nematic LC molecules organize inside the PhC holes. The configuration of the LC director field inside cylindrical capillaries can be indeed numerically obtained by minimizing the total energy of the LCs in contact with the cylinder surface. The molecule anchoring to the lateral surfaces, as well as, for nanometer-size tubes, the balance between the elastic and the surface forces, but also the LC properties (*e.g.* the LC elastic modulus), the cavity geometry, and the sidewall surface (*e.g.* its physical-chemical properties) primarily determine the exact molecule orientation (Burylov, 1991; Crawford et al., 1991a-c; Crawford & Zumer, 1996). Several equilibrium configurations are possible: On one hand, if the anchoring is homeotropic, according to the cylinder diameter and the anchoring force, the planar radial, planar polar or escaped radial configurations can be obtained (see Fig. 13a-c). On the other hand, in the case of a circular anchoring, the planar circular, the circular planar polar or the escaped circular configurations are privileged (see Fig. 13d-f).

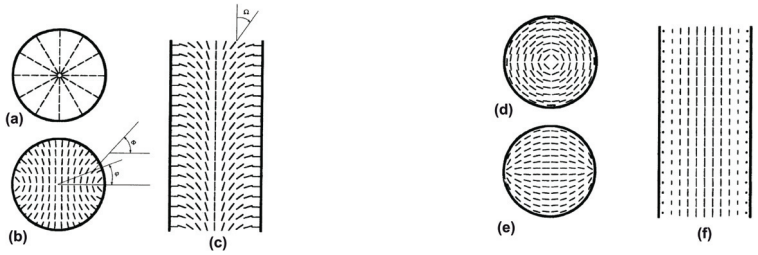

Fig. 13. Examples of liquid crystals director configurations in a cylindrical capillary. (a)-(c) Homeotropic anchoring: (a) planar radial; (b) planar polar; (c) escaped radial. (d)-(f) Circular anchoring: (d) planar circular; (e) circular planar polar; (f) escaped circular (Burylov, 1991).

In infiltrated planar PhCs, the comparison of optical measurements for different polarizations can provide information on the average molecule orientation. We note that all the possible configurations listed above can be grouped into three families: *i*) completely perpendicular (*i.e.* planar), *ii*) completely parallel, or *iii*) escaped (*i.e.* with no dominant orientation): see the inset of Fig. 14. On one hand, for the TM polarization the *E*-field vector is parallel to the hole axis, so that for both LC configurations n_{LC} depends on only one component of the LC dielectric tensor, *i.e.* $n_{LC} = n_e$ and $n_{LC} = n_o$ for the parallel and perpendicular configuration, respectively. On the other hand, for the TE polarization the *E*-field vector lies in the waveguide plane (*i.e.* it is perpendicular to the hole axis). While for

the parallel configuration n_{LC} still depends on only one component of the LC dielectric tensor (*i.e.* $n_{LC} = n_o$), for the perpendicular configuration the average n_{LC} value depends on all the components of the LC dielectric tensor weighted by the local *E*-field. Therefore, it is only for the TM polarization that n_{hole} can be calculated for both LC orientations without any information on the exact director configuration: if $\eta = 0.87$, $n_{hole} = 1.593$ and 1.449 for the parallel and perpendicular configuration, respectively.

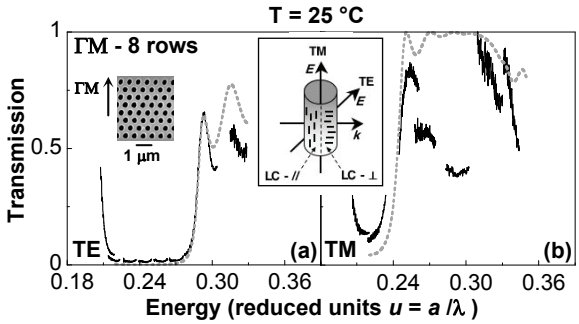

Fig. 14. Measured (black lines) and calculated (grey dotted lines) (a) TE and (b) TM transmission spectra through infiltrated 8-rows thick ΓM-oriented photonic crystal slabs at *T* = 25 °C. The inset shows the *E*-field vector with respect to the light propagation direction (*k*) for both the TE and TM polarizations and the average liquid crystal (LC) orientation parallel (//) and perpendicular (⊥) to the hole axis. (Ferrini et al., 2006).

TE and TM transmission spectra through the infiltrated 8 rows-thick ΓM-oriented PhC slabs (see Sect. 2.1) are shown in Figs. 14a-b, respectively (black lines), for *T* = 25 °C. As in Sects. 3.1-2, the air band transmission edges were fitted by means of a 2D-FDTD model assuming n_{hole} as the free fitting parameter. The calculated spectra are shown in Fig. 14 (grey dotted lines). The fit of the TM spectrum yields $n_{hole} = 1.45$, thus showing that, in contrast to other studies on similar systems (Schuller at al., 2003), most of the LC molecules are aligned perpendicularly to the hole axis (*i.e.* in a planar equilibrium state). This can be due to several factors: the different material system (InP instead of GaAs), the hole shape/surface, etc. We observe that a deeper understanding of the relationship between the n_{hole} values and the molecule orientations may indeed be provided by advanced theoretical calculations taking into account (by means of second-rank tensor indexes) all the possible molecule configurations with respect to the real *E*-field map.

4. Tuning of the optical response of infiltrated planar photonic crystals

4.1 Temperature tuning

As discussed in Sect. 1, the molecular order of LCs infiltrated in planar PhCs can be easily modulated by temperature. When the temperature is increased above the clearing point, the nematic molecular order is destroyed and the LC is in its isotropic phase, where the optical properties are characterized by the isotropic refractive index (n_i).

For instance, transmission spectra through infiltrated FP cavities (see Sect. 2.1) are shown in Fig. 15a for *T* = 25 °C (dotted black line) and *T* = 40 °C (solid black line). The FP resonance energy red-shifts, thus proving the increase of n_{LC} (n_{hole}) with temperature: the fit (see Sect. 3) of the FP resonance at room temperature yields $n_{hole} = 1.47$, *i.e.* for $\eta = 0.87$, $n_{LC} = 1.54$, which

is lower than the isotropic n_i value that is found at 40°C (see Fig. 7). The FP resonance wavelength (λ_{peak}) as a function of temperature is shown in Fig. 15b. For $T \approx 25$ °C λ_{peak} is nearly constant as neither the semiconductor nor the LC refractive indices change significantly. However, due to the increase of n_{LC} (n_{hole}) at the nematic-to-isotropic and nematic-to-polycrystalline LC phase transitions, λ_{peak} sharply increases above 30 °C and below 20 °C with $\Delta\lambda_{peak} = 7$ nm and $\Delta\lambda_{peak} = 11$ nm, respectively. Above 35°C, λ_{peak} remains constant since the increase of the semiconductor refractive index is compensated by the decrease of $n_{LC} = n_i$ with temperature (see Fig. 7). We observe that a symmetrical tuning of the FP resonance is obtained after LC infiltration by either increasing or decreasing the temperature and, for an equal tuning range ΔT, the measured $\Delta\lambda_{peak}$'s are much larger than those obtained by the temperature tuning of similar empty PhC cavities (Wild et al., 2004). However, it is worth noticing that, while tuning rates as low as 10's μs were achieved by locally tuning the temperature of PhC devices (Tinker & Lee, 2005; Chu et al., 2006), response times in order of ms were measured for infiltrated PhC structures (Busch et al., 2004). Finally, the reversibility of the tuning process was verified by cooling down the heated sample to room temperature and checking that the transmission through the FP cavity agreed with the corresponding spectrum measured before heating (Martz et al., 2005). This shows that the complete heating-cooling cycle affects neither the infiltration efficiency (*i.e.* the LC molecules do not evaporate) nor the LC orientation (*i.e.* the hysteresis effects are negligible).

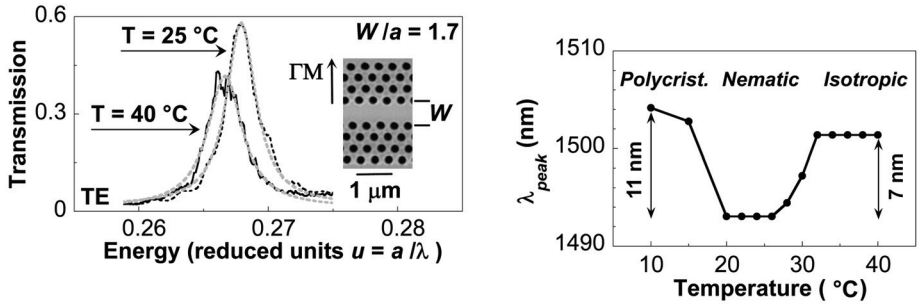

(a) (b)

Fig. 15. (a) Measured transmission spectra through an infiltrated Fabry-Pérot (FP) cavity for T = 25 °C (dotted black line) and T = 40 °C (solid black line). The Airy fits of the resonances are shown (grey dotted lines). The inset: scanning electron microscopy top view of the cavity (W = cavity width). (b) Resonance wavelength (λ_{peak}) as a function of temperature for the infiltrated cavity. The liquid crystal phases are indicated. (Ferrini et al., 2006)

4.2 Electric tuning

As we have briefly discussed in Sect. 1, the optical response of a PhC infiltrated with nematic LCs can be adjusted by applying an external electric field that modifies the molecule orientation inside the holes (Maune et al., 2004; Alagappan et al., 2006; Haurylau et al., 2006a-b; Anderson et al., 2007; Reyes et al. 2008). Since semiconductor materials like InP are usually characterized by small electro-optic coefficients (Scrymgeour et al., 2003), this latter mechanism is particularly interesting when relatively moderate electric fields are used for the tuning of the optical properties of semiconductor-based planar PhCs.

We remark that if the semiconductor heterostructure through which the PhC is etched has a good conductivity (*i.e.* much higher than the LC conductivity), the applied electric field is

screened out of the infiltrated holes where the field distribution results to be nonuniform, so that only a small part of the LC molecules experience a field large enough to reorient. Several approaches have been thus proposed to compensate for these electric-field screening effects and to maximize the electric tunability of the PhC devices, such as deposing the electric contacts or a conducting glass directly on the PhC surface (Maune et al., 2004; Haurylau et al., 2006a-b). Therefore, before setting-up the electric tuning of our infiltrated PhCs, we characterized the electrical conductivity of the InP-based heterostructure (see Sect. 2.1). First of all, four-probe measurements of the current as a function of the applied voltage were used to measure the substrate conductivity: the obtained resistance value $r = 2 \times 10^{-3}\ \Omega \cdot$ cm is due to the *N*-doping of the substrate. Then, the current-voltage characteristics of the heterostructure were measured on two non-patterned samples, one of which was treated with HF to remove the residual SiO_2 over-layer that is usually deposited on the InP surface for the fabrication of planar PhCs (see Sect. 3.1; Mulot et al., 2004). The results of these measurements are reported in Fig. 16. On one hand, for the non-treated sample, the current linearly increases up to 140 V, thus showing a resistance-like behaviour due to the presence of the insulating SiO_2 layer: the measured breakdown voltage (*i.e.* 150 V) indicates a layer thickness in the order of 200 nm. On the other hand, a diode-like characteristics is found for the HF-treated sample: the waveguide heterostructure has a resistance-like behaviour up to 10 V with a minimal electric field intensity inside the guiding layers of 7 V/μm, which is comparable to the critical electric field necessary to induce LC reorentation inside the PhC holes (Halevi et al., 2006).

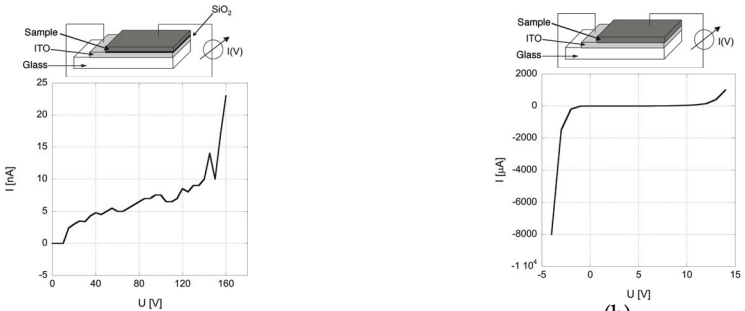

Fig. 16. Measurement of the current-voltage (I-U) characteristics of the InP heterostructures used for the fabrication of planar photonic crystals (see Sect. 2.1) (a) with and (b) without the residual SiO_2 overlayer (El-Kallassi, 2009).

InP-based PhCs similar to those presented in Sect. 2.1 were infiltrated with LCs using the same method as in Sect. 3.1. The infiltration efficiency and the molecule orientation inside the holes were characterized as illustrated in Sect. 3. Differently from what was found in Sect. 3.3, a molecule orientation parallel to the hole axis was found due to a few differences in the PhC fabrication procedure, which may yield different hole morphologies and surface states (*e.g.* rugosity). We remark that, while, when LCs have an equilibrium configuration perpendicular to the hole axis, the application of an electric field parallel to the axis is enough to induce the molecule reorientation (see Fig. 17a), for a purely axial configuration this is not possible. However, if the sample is heated to a temperature close to the clearing point, where the viscosity is reduced and the molecule order is strongly perturbed, the application of an electric field can bring the LCs back to the nematic configuration (see Fig. 17b).

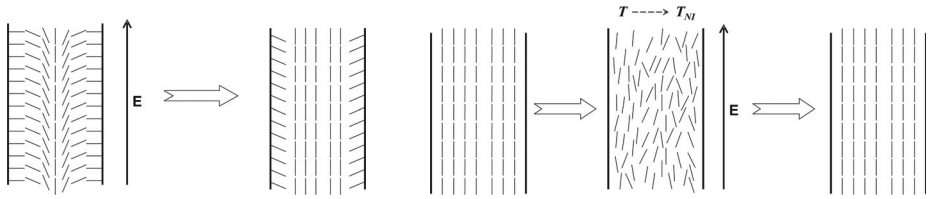

Fig. 17. Sketch of the molecule reorientation induced by an electric field applied along the hole axis when the infiltrated liquid crystals present an equilibrium configuration (a) perpendicular and (b) parallel to the hole axis (El-Kallassi, 2009).

The transmission spectrum through infiltrated FP cavities (see Sect. 2.1) is shown in Fig. 18 (black dotted line) for a temperature T = 32 °C slightly lower than the LC-K15 clearing point (see Sect. 2.2). Due to the application of an electric field (applied tension = +/- 10 V) the FP peak blue-shifts (black dashed line), thus showing a decrease of the hole refractive index n_{hole}. This latter effect is reversible: when switching off the electric field (applied tension = 0 V), the peak comes back to its initial location (grey dashed line). Even without a complete analysis of the LC orientation inside the holes, the decrease of n_{hole} clearly indicates a LC reorentation parallel to the hole axis. Therefore, the possibility of electrically tuning the optical properties of InP-based PhCs infiltrated with nematic LCs is thouroughly demonstrated.

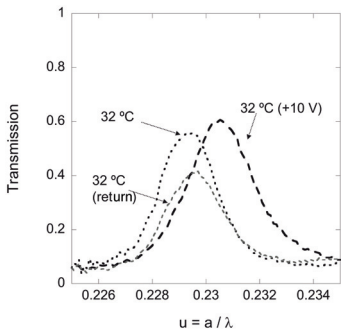

Fig. 18. Measured transmission spectra through an infiltrated Fabry-Pérot (FP) cavity for T = 32 °C (black dotted line) with and without an applied electric field (see Fig. 17): the black and grey dashed lines correspond to an applied voltage V = +/- 10 V and 0 V (return), respectively (El-Kallassi, 2009).

4.3 Optical tuning

In order to optically tune the response of infiltrated planar PhCs, a photo-responsive LC blend was used that consists of nematic LC-K15 as host molecules and 4-butyl-4'-methoxyazobenzene (BMAB) as guest molecules (see Fig. 19a).

BMAB is an azobenzene derivative that possesses an alkoxy substituent and a butyl group at the para positions of the azobenzene. It has a liquid crystalline behavior with a nematic-isotropic phase transition temperature at T_{NI}(BMAB) = 45 °C and a polycrystalline-nematic phase transition temperature at T_{KN}(BMAB) = 35 °C. Azobenzene molecules can undergo a

reversible photo-isomerization between their trans (rodlike shape) and cis (bent shape) molecular forms upon irradiation with UV and visible light. In Fig. 19b, the measured absorption spectra of the BMAB trans and cis forms are shown. The trans-isomer has a main absorption band in the UV around 350 nm (π-π* molecular transition), whilst the cis-isomer has an absorption peak in the visible around 450 nm (*n*-π* molecular transition). We remark that the absorption band of the host LC-K15 is located in the UV around 280 nm and does not overlap with those of the BMAB (Legge & Mitchell, 1992). The trans-isomer, which is the thermally stable ground state, can transform into the cis-isomer by absorbing UV light, and the cis-isomer can return to the trans-isomer form either by visible light irradiation or by thermal isomerization. The photo-isomerization reactions have time scales on the order of ps's, while without illumination, the cis form will thermally reconvert to the more stable trans form with a lifetime that, for azobenzenes, is typically on the order of hours (Yager & Barret, 2006). On one hand, upon UV irradiation, a steady state can be reached where 100% of the trans molecules are converted to the cis form. On the other hand, since the *n*-π* band is present in the absorption spectra of both isomers, irradiating a photochromic mixture with visible light will bring the system in a photostationary state, whose composition is based on the competition among the photo-isomerization rates and the thermal decay rate: thus, a 100% cis-to-trans photo-conversion is not possible and the resulting mixture comprises both molecular forms.

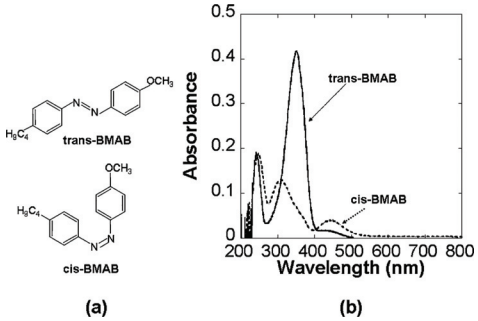

Fig. 19. (a) Chemical structures of the trans and the cis molecular forms of the azobenzene derivative [4-butyl-4'-methoxyazobenzene (BMAB)]; (b) Measured absorption spectra of the BMAB trans (full curve) and cis (broken curve) forms (El-Kallassi et al., 2007).

The phase transitions in a mixture of LC-K15 doped with BMAB are shown in Figs. 20 and 21 as a function of the BMAB mole fraction ρ (Legge & Mitchell, 1992). In Fig. 20a, the nematic-isotropic phase transition temperature T_{NI} is plotted as a function of ρ for a mixture where all the BMAB molecules are in the trans form, *i.e.* before UV irradiation. Due to its rod-like molecular shape, the trans form stabilizes the LC nematic phase and T_{NI} increases gradually with ρ. Once the mixture is irradiated with UV light and the trans-to-cis photo-isomerization takes place, the bent shape of the cis isomer introduces molecular disorder in the mixture. Therefore, T_{NI} is lowered and its decrease is proportional to the concentration of the cis-isomer. In Fig. 20b, the lowered temperature value T^*_{NI} is plotted as a function of ρ for 100% of the BMAB molecules in the cis form. If the system is held at a temperature between T_{NI} and T^*_{NI}, due to the trans-cis photo-isomerization of the guest BMAB molecule, the nematic-isotropic phase transition of the LC host can be induced isothermally. In the equilibrium phase, the BMAB molecules are in the trans-form and the system is globally in

the nematic phase. Upon irradiation with UV light, the photo-isomerization trans-cis brings the system into the isotropic phase. A complete photo-isomerization is not necessary to induce the nematic-to-isotropic transition and response times on the order of ms's can be achieved depending on the BMAB concentration, the temperature, and the irradiation power (Kubo et al., 2005). If the temperature is close to T^*_{NI} the system may show a biphasic behavior (Legge & Mitchell, 1992): while no phase separation is observed for mixtures of LC-K15 doped with BMAB, a phase separation between domains of nematic and isotropic LC-K15+cis-isomers occurs (see Fig. 20b). The photo-induced nematic-isotropic transition is reversible: irradiation with visible light brings part of the cis-isomers back to the trans-form and the system back to its nematic phase. This reverse transition has response times on the order of several 10's seconds up to minutes depending on the temperature and on the percentage of the cis-isomer in the mixture. Finally, if the temperature is close to T_{NI} the system may fall into the photo-stationary state described above and the nematic phase cannot be reached simply by visible light irradiation because the trans-cis and cis-trans photo-isomerization rates are similar. The system is a ternary mixture (LC-K15+cis- and trans-isomers) with a phase transition temperature T_{NI}(PS) lower than T_{NI} (see Fig. 20c).

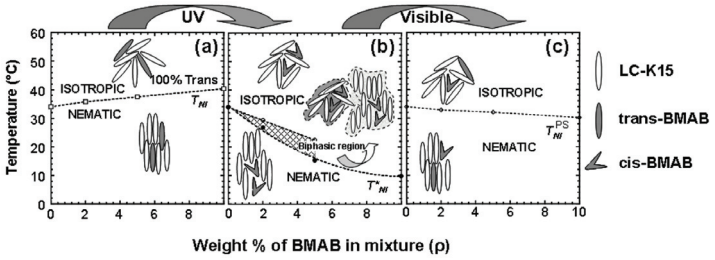

Fig. 20. Phase diagram of the LC-K15/BMAB mixture as a function of the BMAB mole fraction ρ (Legge & Mitchell, 1992). (a) 100% of the BMAB molecules are in the trans form; (b) 100% of the BMAB molecules are in the cis form: the shaded region is the biphasic region; (c) The photostationary state after white light irradiation. $T_{NI,}$ T^*_{NI} and T_{NI}(PS) are the corresponding nematic-isotropic transition temperatures (El-Kallassi et al., 2007).

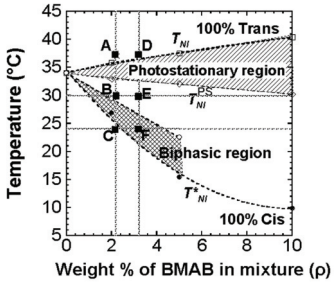

Fig. 21. Complete phase diagram of the LC-K15/BMAB mixture. The photostationary region is hashed. The experimental conditions chosen for the infiltration and the optical tuning of PhCs are indicated (black squares) (El-Kallassi et al., 2007).

The complete phase diagram of the LC-K15/BMAB mixture is summarized in Fig. 21. On one hand, due to the widening of the photo-stationary region with increasing ρ, the BMAB concentration in the mixture must remain well below 10% if one wants to preserve the complete photo-reversibility of the host-guest mixture (Kubo et al., 2005). On the other hand, working conditions close to the photo-stationary limit may shorten the response times of the system. Mixtures with ρ = 2.2% and 3.2% were prepared. The transition temperature T^*_{NI} is expected to be 5 °C and 7 °C lower than T_{NI} for the 2.2% and 3.2% mixtures, respectively (see Fig. 20). The photo-stationary state is calculated to be located at about 2 °C below T_{NI}.
As in Sect. 3, an infiltration efficiency η = 0.93 was found by measuring the transmission spectra at a temperature well above the clearing point of the LC-K15/BMAB mixtures (*i.e.* T = 37 °C). On the other hand, the fit of the experimental transmission spectra at room temperature yields an average molecule orientation parallel to the hole axis (see Sect. 4.2).

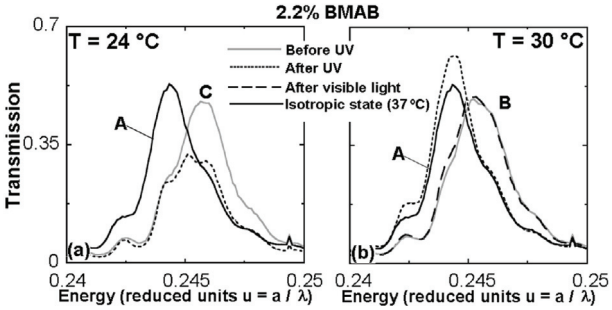

Fig. 22. Measured TE transmission spectra through a Fabry-Perot cavity (W/a = 1.8) infiltrated with a LC-K15/BMAB mixture (ρ = 2.2%), before (grey lines) and after irradiation with UV (dotted lines) and visible light (dashed line), (a) at 24 °C and (b) 30 °C. The spectrum for to T = 37 °C is represented as reference (black line) (El-Kallassi et al., 2007).

The TE polarized transmission spectra through an infiltrated FP cavity for ρ = 2.2% at temperatures T = 24 °C and 30 °C (points C and B in Fig. 21) are shown in Figs. 22a-b, respectively. The spectra before and after UV irradiation, and after a subsequent irradiation with visible light are reported (grey, dotted and dashed curves, respectively). The spectrum measured at T = 37 °C (point A in Fig. 21) is shown as reference (black solid curve). At T = 37 °C, since $T > T_{NI}$, the LC-15/BMAB mixture is always in the thermal-isotropic phase even when 100% of trans-isomers are present. Thus, the FP resonance red-shifts with respect to the lower temperatures (nematic phase). Light irradiation has no effect at T = 24 °C: since $T < T^*_{NI}$, the system remains in its nematic phase even after a complete photo-isomerization and the shift of the FP resonance after UV irradiation is negligible. At T = 30 °C ($T^*_{NI} < T < T_{NI}$) after UV irradiation the resonance peak shifts of the same amount as for T = 37 °C: a complete nematic-to-isotropic phase transition is obtained isothermally by light irradiation (photo-isotropic state). Finally, after visible light irradiation, the FP peak blue-shifts to its original position, thus showing the reversibility of the photo-induced phase transition. We remark that response times on the order of ms's to s's might be achieved depending on the BMAB concentration, the temperature, and the irradiation power.

5. Conclusion

In conclusion, we have demonstrated that the combination of semiconductor-based photonic devices with nematic liquid crystals can enable the fabrication of new hybrid structures with increased functionalities. In particular, a reproducible and reliable infiltration procedure for planar PhCs has been developed and systematically validated through optical measurements. With respect to previous studies, this technique allows the accurate control of all the infiltration parameters (*i.e.* temperature and pressure) and, when necessary, the functionalization of the PhC surface. An accurate method based on in-situ optical measurements as a function of temperature and polarization was developed to characterize the infiltration efficiency and the molecule equilibrium organization inside the PhC holes. The temperature, electric and optical tuning of the infiltrated PhC devices were demonstrated. In spite of their slow response time with respect to other tuning approaches (see Sect. 1), PhC devices infiltrated with LCs can be envisaged for reconfiguration applications, switching between different functionalities and adjustment of filter devices. Moreover, recent studies have shown that the selective filling of few holes instead of the whole device further amplifies the potential of PhC infiltration (El-Kallassi et al., 2008). On one hand, the local filling allows one to overcome the decrease of the device performances (*e.g.* the cavity quality factor: see Sect. 3) when the PhC is globally infiltrated due to the reduction of the refractive index contrast between the hole array and the semiconductor matrix. On the other hand, the selective infiltration of few holes can provide an alternative approach for integrated photonic components (Mingaleev et al., 2004; Erickson et al., 2006; Intonti et al., 2006; Tomljenovic-Hanic et al., 2006; Smith et al., 2007; Faraon et al., 2008).

The author thanks Dr. P. El-Kallassi and Prof. L. Zuppiroli from the Ecole Polytechnique Fédérale de Lausanne (Switzerland) for their fundamental contribution to this work. The PhC samples were fabricated within the framework of the EU project Photonic Crystal Integrated Circuits (PCIC) and the EU Network of Excellence on Photonic Integrated Components and Circuits (ePIXnet). The infiltration experiments were performed within the framework of the Swiss National Center of Competence in Research (NCCR) in Quantum Photonics.

6. References

Alagappan, G.; Sun, X.W.; Yu, M.B. & Shum, P. (2006). Controllable polarization splitting in liquid crystal infiltrated phtonic crystals. *Proceedings of SPIE - Photonic Crystal Materials and Devices IV*, Vol. 6128, pp. 61280H-1, San Jose CA, USA, January 2006, SPIE, Bellingham WA

Anderson, S.P.; Haurylau, M.; Zhang, J. & Fauchet, P.M. (2007). Hybrid photonic crystal microcavity switches on SOI. *Proceedings of SPIE - Silicon Photonics II*, Vol. 6477, pp. 647712-1, San Jose CA, USA, January 2007, SPIE, Bellingham WA

Asakawa, K.; Sugimoto, Y.; Watanabe, Y.; Ozaki, N.; Mizutani, A.; Takata, Y.; Kitagawa, Y.; Ishikawa, H.; Ikeda, N.; Awazu, K.; Wang, X.; Watanabe, A.; Nakamura, S.; Ohkouchi, S.; Inoue, K.; Kristensen, M.; Sigmund, O.; Ingo Borel, P. & Baets, R. (2006). Photonic crystals and quantum dots technologies for all-optical switch and logic device. *New Journal of Physics*, Vol. 8, 208

Baba, T.; Shiga, M.; Inoshita, K. & Koyama, F. (2003). Carrier plasma shift in GaInAsP photonic crystal point defect cavity. *Electronics Letters*, Vol. 39, No. 21, 1516 - 1518

Barthelemy, P.; Ghulinyan, M.; Gaburro, Z.; Toninelli, C.; Pavesi, L. & Wiersma, D. (2007). Optical switching by capillary condensation. *Nature Photonics*, Vol. 1, 172-175

Belotelov, V.I. & Zvezdin, A.K. (2005). Magneto-optical properties of photonic crystals. *Journal of the Optical Society of America B*, Vol. 22, No. 1, 286-292

Bristow, A.D.; Kundys, D.O.; García-Déniz, A.Z.; Wells, J.-P. R.; Fox, A.M.; Skolnick, M.S.; Whittaker, D.M.; Tahraoui, A.; Krauss, T.F. & Roberts, J.S. (2006). Enhanced all-optical tuning of leaky eigenmodes in photonic crystal waveguides. *Optics Letters*, Vol. 31, No. 15, 2284-2286

Brugioni, S.; Meucci, R. & Faetti, S. (2006). Refractive indices of liquid crystals E7 and K15 in the mid- and near-IR regions. *Journal of Optical Technology*, Vol. 73, No. 5, 315-317

Burylov, S.V. (1997). Equilibrium configuration of a nematic liquid crystal confined to a cylindrical cavity. *JETP*, Vol. 85, No. 5, 873–886

Busch, K. & John, S. (1999). Liquid-crystal photonic-band-gap materials: the tunable electromagnetic vacuum. *Physical Review Letters*, Vol. 83, No. 5, 967-970

Busch, K.; Lölkes, S.; Wehrspohn, R.B. & Föll, H. (2004). *Photonic Crystals*, Wiley-VCH, ISBN 3-527-40432-5, Weinheim

Chu, T.; Yamada, H.; Gomyo, A.; Ushida, J.; Ishida, S. & Arakawa, Y. (2006). Tunable optical notch filter realized by shifting the photonic bandgap in a silicon photonic crystal line-defect waveguide. *IEEE Photonics Technology Letters*, Vol. 18, No. 24, 2614–2616

Crawford, G.P.; Vilfan, M.; Doane, J.W. & Vilfan, I. (1991a). Escaped-radial nematic configuration in submicrometer-size cylindrical cavities : Deuterium nuclear-magnetic-resonance study. *Physical Review A*, Vol. 43, No. 2, 835–842

Crawford, G.P.; Allender, D.W.; Doane, J.W.; Vilfan, M. & Vilfan, I. (1991b). Finite molecular anchoring in the escaped-radial nematic configuration : A 2 NMR study. *Physical Review A*, Vol. 44, No. 4, 2570–2577

Crawford, G.P.; Stannarius, R. & Doane, J.W. (1991c). Surface-induced orientational order in the isotropic phase of a liquid-crystal material. *Physical Review A*, Vol. 44, No. 4, 2558–2569

Crawford, G.P. & Zumer, S. (1996). *Liquid Crystals in Complex Geometries*, Taylor & Francis, ISBN 0-203-21107-3, London

Du, F. ; Lu, Y.-Q. & Wu, S.-T. (2004). Electrically tunable liquid-crystal photonic crystal fiber. *Applied Physics Letters*, Vol. 85, No. 12, 2181-2183

El-Kallassi, P.; Ferrini, R.; Zuppiroli, L.; Le Thomas, N.; Houdré, R.; Berrier, A.; Anand, S. & Talneau, A. (2007). Optical tuning of planar photonic crystals infiltrated with organic molecules. *Journal of the Optical Society of America B*, Vol. 24, No. 9, 2165-2171

El-Kallassi, P.; Balog, S.; Houdré, R.; Balet, L.; Li, L.; Francardi, M.; Gerardino, A.; Fiore, A.; Ferrini, R. & Zuppiroli, L. (2008). Local infiltration of planar photonic crystals with UV-curable polymers. *Journal of the Optical Society of America B*, Vol. 25, No. 10, 1562-1567

El-Kallassi, P. (2009). *Thesis: Accordabilité de la réponse optique des cristaux photoniques par infiltration de matériaux organiques* (http://library.epfl.ch/en/theses/?nr=4343), EPFL, Lausanne

Erickson, D.; Rockwood, T.; Emery, T.; Scherer, A. & Psaltis, D. (2006). Nanofluidic tuning of photonic crystal circuits. *Optics Letters*, Vol. 31, No. 1, 59-61

Faraon, A.; Englund, D.; Bulla, D.; Luther-Davies, B.; Eggleton; B.J.; Stoltz, N.; Petroff, P. & Vučković, J. (2008). Local tuning of photonic crystal cavities using chalcogenide glasses. *Applied Physics Letters*, Vol. 92, No. 4, 043123

Ferrini, R.; Lombardet, B.; Wild, B.; Houdré, R.; Olivier, S.; Benisty, H.; Djoudi, A.; Legouézigou, L.; Hubert, S.; Sainson, S.; Chandouineau, J.-P.; Fabre, S., Pommereau, F. & Duan, G.-H. (2002a). Optical characterisation of 2D InP-based photonic crystals fabricated by inductively coupled plasma etching. *Electronics Letters*, Vol. 38, No. 17, 962-964

Ferrini, R.; Leuenberger, D.; Mulot, M.; Qiu, M.; Moosbürger, J.; Kamp, M.; Forchel, A.; Anand, S. & Houdré, R. (2002b). Optical study of two-dimensional InP-based photonic crystals by internal light source technique. *IEEE Journal of Quantum Electronics*, Vol. 38, No. 7, 786-799

Ferrini, R.; Lombardet, B.; Wild, B.; Houdré, R. & Duan, G-H. (2003a). Hole depth- and shape-induced radiation losses in two-dimensional photonic crystals. *Applied Physics Letters*, Vol. 82, No. 7, 1009-1011

Ferrini, R.; Houdré, R.; Benisty, H.; Qiu, M. & Moosburger, J. (2003b). Radiation losses in planar photonic crystals : two-dimensional representation of hole depth and shape by an imaginary dielectric constant. *Journal of the Optical Society of America B*, Vol. 20, No. 3, 469-478

Ferrini, R.; Berrier, A.; Dunbar, L.A.; Houdré, R.; Mulot, M.; Anand, S.; de Rossi, S. & Talneau, A. (2004). Minimization of out-of-plane losses in planar photonic crystals by optimising the vertical waveguide. *Applied Physics Letters*, Vol. 85, No. 18, 3998-4000

Ferrini, R.; Martz, J.; Zuppiroli, L.; Wild, B.; Zabelin, V.; Dunbar, L.A.; Houdré, R.; Mulot, M. & Anand, S. (2006). Planar photonic crystals infiltrated with liquid crystals: tuning and optical characterization of molecule orientation. *Optics Letters*, Vol. 31, No. 9, 1238-1240

Gottardo, S.; Wiersma, D.S. & Vos, W.L. (2003). Liquid crystal infiltration of complex dielectrics. *Physica B*, Vol. 338, No. 1, 143-148

Grüning, U.; Lehmann, V.; Ottow, S. & Busch, K. (1995). Macroporous silicon with a complete two-dimensional photonic band gap centered at 5 μm. *Applied Physics Letters,* Vol. 68, No. 6, 747-749

Haché, A. & Bourgeois, M. (2000). Ultrafast all-optical switching in a silicon-based photonic crystal. *Applied Physics Letters,* Vol. 77, No. 25, 4089-4091

Halevi, P.; Reyes-Avendaño, J.A. & Reyes-Cervantes, J. A. (2006). Electrically tuned phase transition and band structure in a liquid-crystal-infilled photonic Crystal. *Physical Review E*, Vol. 73, N. 4, 040701

Haurylau, M.; Anderson, S.P.; Marshall, K.L. & Fauchet, P.M. (2006a). Electrically tunable silicon 2-D photonic bandgap structures. *IEEE Journal of Selected Topics in Quantum Electronics*, Vol. 12, No. 6, 1527-1533

Haurylau, M.; Anderson, S.P.; Marshall, K.L. & Fauchet, P.M. (2006b). Electrical modulation of silicon-based two-dimensional photonic bandgap structures. *Applied Physics Letters*, Vol. 88, No. 6, 061103

Hu, X.; Jiang, P.; Yang, H. & Gong, Q. (2006). All-optical tunable photonic bandgap microcavities with a femtosecond time response. *Optics Letters*, Vol. 31, No. 18, 2777-2779

Hu, X.; Jiang, P.; Ding, C. & Gong, Q. (2007). All-optical tunable narrow-band organic photonic crystal filters. *Applied Physics B*, Vol. 87, No. 2, 255-258

Ikeda, T. (2003). Photomodulation of liquid crystal orientations for photonic applications. *Journal of Materials Chemistry*, Vol. 13, 2037-2057

Intonti, F.; Vignolini, S.; Türck, V.; Colocci, M.; Bettotti, P.; Pavesi, L.; Schweizer, S.L.; Wehrspohn, R. & Wiersma, D. (2006). Rewritable photonic circuits. *Applied Physics Letters*, Vol. 89, No. 21, 211117

Joannopolous, J.D.; Johnson, S.G.; Winn, J.N. & Meade, R.D. (2008). *Photonic Crystals: Molding the Flow of Light – Second Edition*, Princeton University Press, ISBN 978-0-691-12456-8, Princeton

Kanamori, Y.; Kitani, T. & Hane, K. (2007). Control of guided resonance in a photonic crystal slab using microelectromechanical actuators. *Applied Physics Letters*, Vol. 90, No. 3, 031911

Kang, D.; Maclennan, J.E.; Clark, N.A.; Zakhidov, A.A. & Baughman, R.H. (2001). Electro-optic behaviour of liquid-crystal-filled silica opal photonic crystals: effect of liquid-crystal alignment. *Physical Review Letters*, Vol. 86, No. 18, 4052-4055

Kee, C.-S.; Kim, J.-E.; Park, H.Y.; I. Park & Lim, H. (2000). Two-dimensional tunable magnetic photonic crystals. *Physical Review B*, Vol. 61, No. 23, 15523-15525

Kosmidou, E.P.; Kriezis, E.E. & Tsiboukis, T.D. (2005). Analysis of tunable photonic crystal devices comprising liquid crystal materials as defects. *IEEE Journal of Quantum Electronics*, Vol. 41, No. 5, 657-665

Kubo, S.; Gu, Z.-Z.; Takahashi, K.; Ohko, Y.; Sato, O. & Fujishima, A. (2002). Control of the optical band structure of liquid crystal infiltrated inverse opal by a photoinduced nematic−isotropic phase transition. *Journal of the American Chemical Society*, Vol. 124, No. 37, 10950-10951

Kubo, S.; Gu, Z.-Z.; Takahashi, K.; Fujishima, A.; Segawa, H. & Sato, O. (2004). Tunable photonic band gap crystals based on a liquid crystal-infiltrated inverse opal structure. *Journal of the American Chemical Society*, Vol. 126, No. 26, 8314-8319

Kubo, S.; Gu, Z.-Z.; Takahashi, K.; Fujishima, A.; Segawa, H. & Sato, O. (2005). Control of the optical properties of liquid crystal-infiltrated inverse opal structures using photo irradiation and/or an electric field. *Chemistry of Materials*, Vol. 17, No. 9, 2298-2309

Legge, C.H. & Mitchell, G.R. (1992). Photo-induced phase transitions in azobenzene-doped liquid crystals. *Journal of Physics D: Applied Physics*, Vol. 25, No. 3, 492-499

Leonard, S.W.; Mondia, S.W.; van Driel, H.M.; Toader, O.; John, S.; Busch, K.; Birner, A.; Gösele, U. & Lehmann, V. (2000). Tunable two-dimensional photonic crystals using liquid crystal infiltration. *Physical Review B*, Vol. 61, No. 4, R2389-R2392

Leonard, S.W.; van Driel, H.M.; Schilling, J. & Wehrspohn, R.B. (2002). Ultrafast band-edge tuning of a two-dimensional silicon photonic crystal via free-carrier injection. *Physical Review B*, Vol. 66, No. 16, 161102-161105

Li, J. & Wu, S.-T. (2004). Extended Cauchy equations for the refractive indexes of liquid crystals. *Journal of Applied Physics*, Vol. 95, No. 3, 896-901

Lourtioz, J.M.; Benisty, H.; Berger, V.; Gérard, J.M.; Maystre, D. & Tchelnokov, A. (2005). *Photonic Crystals*, Springer-Verlag, ISBN 3-540-24431-X, Berlin Heidelberg

Lyubchanskii, I.L.; Dadoenkova, N.N.; Lyubchanskii, M.I.; Shapovalov, E.A. & Rasing, Th. (2003). Magnetic photonic crystals. *Journal of Physics D: Applied Physics*, Vol. 36, No. 18, R277-R287

Mansare, J.T.; Decressain, R.; Gors, C. & Dolganov, V.K. (2002). Phase transformations and dynamics of 4-cyano-4'-pentylbiphenyl (5CB) by nuclear magnetic resonance, analysis differential scanning calorimetry, and wide-angle X-ray diffraction analysis. *Molecular Crystals and Liquid Crystals Science and Technology A: Molecular Crystals and Liquid Crystals*, Vol. 382, 97-111

Märki, I.; Salt, M. & Herzig, H.P. (2006). Tuning the resonance of a photonic crystal microcavity with an AFM probe. *Optics Express*, Vol. 14, No. 7, 2969-2978

Marroum, R.-M.; Iannacchione, G.S.; Finotello, D. & Lee, M.A. (1995). Numerical study of cylindrically confined nematic liquid crystals. *Physical Review E*, Vol. 51, No. 4, R2743-R2746

Martz, J.; Zuppiroli, L. & Nüesch, F. (2004). Benzoic and aliphatic carboxylic acid monomolecular layers on oxidized GaAs surface as a tool for two-dimensional photonic crystal infiltration. *Langmuir* Vol. 20, No. 26, 11428-11432

Martz, J.; Wild, B.; Ferrini, R.; Dunbar, L.A.; Mulot, M.; Anand, S.; Houdré, R. & Zuppiroli, L. (2005). Tuning the optical properties of planar photonic crystals by liquid crystal infiltration. *Proceedings of SPIE - Tuning the Optical Response of Photonic Bandgap Structures II*, Vol. 5926, pp. 592601-1, San Diego CA, USA, August 2005, SPIE, Bellingham WA

Martz, J.; Ferrini, R.; Nüesch, F.; Zuppiroli, L.; Wild, B.; Dunbar, L.A.; Houdré, R.; Mulot, M. & Anand, S. (2006). Liquid crystal infiltration of InP-based planar photonic crystals. *Journal of Applied Physics*, Vol. 99, No. 10, 103105

Maune, B.; Loncar, M.; Witzens, J.; Hochberg, M.; Baehr-Jones, T.; Psaltis, D.; Scherer, A. & Qiu, Y. (2004). Liquid-crystal electric tuning of a photonic crystal laser. *Applied Physics Letters*, Vol. 85, No. 3, 360-362

Maune, B.; Witzens, J.; Baehr-Jones, T.; Kolodrubetz, M.; Atwater, H.; Scherer, A.; Hagen, R. & Qiu, Y. (2005). Optically triggered Q-switched photonic crystal laser. *Optics Express*, Vol. 13, No. 12, 4699-4707

Mertens, G.; Röder, T.; Schweins, R.; Huber, K. & Kitzerow, H.-S. (2002). Shift of the photonic band gap in two photonic crystal/liquid crystal composites. *Applied Physics Letters*, Vol. 80, No. 11, 1885-1887

Mertens, G.; Röder, T.; Matthias, H.; Marsmann, H.; Kitzerow, H.-S.; Schweizer, S.L.; Jamois, C.; Wehrspohn, R.B. & Neubert, M. (2003). Two- and three-dimensional photonic crystals made of macroporous silicon and liquid crystals. *Applied Physics Letters* Vol. 83, No. 15, 3036-3038

Mingaleev, S.; Schillinger, M.; Hermann, D. & Busch, K. (2004). Tunable photonic crystal circuits: concepts and designs based on single-pore infiltration. *Optics Letters*, Vol. 29, No. 24, 2858-2860

Mulot, M.; Ferrini, R.; Wild, B.; Moosburger, J.; Forchel, A.; Houdré, R. & Anand, S. (2004). Fabrication of two-dimensional InP-based photonic crystals by chlorine based chemically assisted ion beam etching. *Journal of Vacuum Science & Technology B*, Vol. 22, No. 2, 707-709

Myers, D. (1991). *Surfaces, Interfaces and Colloids*, Wiley-VCH, ISBN 0471330604, Weinheim

Ndi, F.C.; Toulouse, J.; Hodson, T. & Prather, D.W. (2005). All-optical switching in silicon photonic crystal waveguides by use of the plasma dispersion effect. *Optics Letters*, Vol. 30, No. 17, 2254-2256

Ndi, F.C.; Toulouse, J.; Hodson, T. & Prather, D.W. (2006). Optically tunable silicon photonic crystal microcavities. *Optics Express*, Vol. 14, No. 11, 4835-4841

Nielsen, K.; Noordegraaf, D.; Sørensen, T.; Bjarklev, A. & Hansen, T.P. (2005). Selective filling of photonic crystal fibres. *Journal of Optics A: Pure Applied Optics*, Vol. 7, No. 8, L13-L20

Qiu, M.; Jaskorzynska, B.; Swillo, M. & Benisty, H. (2002). Time-domain 2D modeling of slab-waveguide based photonic-crystal devices in the presence of radiation losses. *Microwave and Optical Technology Letters*, Vol. 34, No. 5, 387-393

Raineri, F.; Cojocaru, C.; Raj, R.; Monnier, P.; Levenson, A.; Seassal, C.; Letartre, X. & Viktorovitch, P. (2005). Tuning a two-dimensional photonic crystal resonance via optical carrier injection. *Optics Letters*, Vol. 30, No. 1, 64-66

Reyes, J.A.; Reyes-Avendaño, J.A. & Halevi, P. (2008). Electrical tuning of photonic crystals infilled with liquid crystals. *Optics Communications* Vol. 281, No. 9, 2535–2547

Shimoda, Y.; Ozaki, M. & Yoshino, K. (2001). Electric field tuning of a stop band in a reflection spectrum of synthetic opal infiltrated with nematic liquid crystal. *Applied Physics Letters*, Vol. 79, No. 22, 3627-3629

Schuller, Ch.; Klopf, F.; Reithmaier, J.P.; Kamp, M. & Forchel, A. (2003). Tunable photonic crystals fabricated in III-V semiconductor slab waveguides using infiltrated liquid crystals. *Applied Physics Letters*, Vol. 82, No. 17, 2767-2769

Scrymgeour, D.; Malkova, N.; Kim, S. & Gopalan, V. (2003). Electro-optic control of the superprism effect in photonic crystals. *Applied Physics Letters*, Vol. 82, No. 19, 3176-3178

Smith, C.L.C.; Wu, D.K.C.; Lee, M.W.; Monat, C.; Tomljenovic-Hanic, S.; Grillet, C.; Eggleton, J.; Freeman, D.; Ruan, Y.; Madden, S.; Luther-Davies, B.; Giessen, H. & Lee, Y-H. (2007). Microfluidic photonic crystal double heterostructure. *Applied Physics Letters*, Vol. 91, No. 12, 121103

Song, B-S.; Noda, S.; Asano, T. & Akahane, Y. (2005). Ultra-high-Q photonic double-. heterostructure nanocavity. *Nature Materials*, Vol. 4, No. 3, 207-210

Sugimoto, Y.; Tanaka, Y.; Ikeda, N.; Nakamura, Y.; Asakawa, K. & Inoue, K. (2004). Low propagation loss of 0.76 dB/mm in GaAs-based single-line-defect two-dimensional photonic crystal slab waveguides up to 1 cm in length. *Optics Express*, Vol. 12, No. 6, 1090-1096

Sung, J.-H.; Hirano, S.; Tsutsumi, O.; Kanazawa, A.; Shiono, T. & Ikeda, T. (2002). Dynamics of photochemical phase transition of guest/host liquid crystals with an azobenzene derivative as a photoresponsive chromophore. *Chemistry of Materials*, Vol. 14, No. 1, 385-391

Takeda, H. & Yoshino, K. (2003). Tunable light propagation in Y-shaped waveguides in two-dimensional photonic crystals composed of semiconductors depending on temperature. *Optics Communications,* Vol. 219, No. 1-6, 177-182

Tanabe, T.; Nishiguchi, K.; Shinya, A.; Kuramochi, E.; Inokawa, H.; Notomi, M.; Yamada, K.; Tsuchizawa, T.; Watanabe, T.; Fukada, H.; Shinoijma, H. & Itabashi, S. (2007). Fast all-optical switching using ion-implanted silicon photonic crystal nanocavities. *Applied Physics Letters,* Vol. 90, No. 3, 031115

Tay, S.; Thomas, J.; Momeni, B.; Askari, M.; Adibi, A.; Hotchkiss, P.J.; Jones, S.C.; Marder, S.R.; Norwood, R.A. & Peyghambarian, N. (2007). Planar photonic crystals infiltrated with nanoparticle/polymer composites. *Applied Physics Letters*, Vol. 91, No. 22, 221109

Teo, S.H.G.; Liu, A.Q.; Zhang, J.B. & Hong, M.H. (2006). Induced free carrier modulation of photonic crystal optical intersection via localized optical absorption effect. *Applied Physics Letters,* Vol. 89, No. 9, 091910

Tinker, M.T. & Lee, J.-B. (2005). Thermo-optic photonic crystal light modulator. *Applied Physics Letters,* Vol. 86, No. 22, 221111

Tomljenovic-Hanic, S.; Martijn de Sterke, C. & Steel, M.J. (2006). Design of high-Q cavities in photonic crystal slab heterostructures by air-holes infiltration. *Optics Express*, Vol. 14, No. 25, 12451-12456

van der Heijden, R.; Carlström, C-F.; Snijders, J.; van der Heijden, R.W.; Karouta, F.; Nötzel, R.; Salemink, H.; Kjellander, C.; Bastiaansen, C.; Broer, D. & van der Drift, E. (2006a). InP-based two-dimensional photonic crystals filled with polymers. *Applied Physics Letters*, Vol. 88, No. 16, 161112

van der Heijden, R.; Kjellanderb, C.; Carlströma, C.F.; Snijders, J.; Kickena, H.; van der Heijden, R.W.; Cees Bastiaansen, C.; Broerc, D.; Karoutaa, F.; Nötzel, R.; van der Driftd, E. & Salemink, H. (2006b). InP-based planar photonic crystals infiltrated with solid polymers and liquid crystals. *Proceedings of* SPIE - *Tuning the Optic Response of Photonic Bandgap Structures III*, Vol. 6322, pp. 632205-1, San Diego CA, USA, August 2006, SPIE, Bellingham WA

Vlasov, Y.A.; Bo, X-Z.; Sturm, J.C. & Norris, D.J. (2001). On-chip natural assembly of silicon photonic bandgap crystals. *Nature*, Vol. 414, No. 6861, 289-293

Yoshino, K.; Shimoda, Y.; Kawagishi, Y.; Nakayama, K. & Ozaki, M. (1999b). Temperature tuning of the stop band in transmission spectra of liquid-crystal infiltrated synthetic opal as tunable photonic crystal. *Applied Physics Letters*, Vol. 75, No. 7, 932-934

Weiss, S.M. & Fauchet, P.M. (2003). Electrically tunable porous silicon active mirrors. *Physica Status Solidi (a)*, Vol. 197, No. 2, 556-560

Weiss, S.M.; Ouyang, H.; Zhang, J. & Fauchet, P.M. (2005a). Electrical and thermal modulation of silicon photonic bandgap microcavities containing liquid crystals. *Optics Express*, Vol. 13, No. 4, 1090-1097

Weiss, S.M.; Haurylau, M. & Fauchet, P.M. (2005b). Tunable photonic bandgap structures for optical interconnects. *Optical Materials*, Vol. 27, No. 5, 740-744

Wild, B.; Ferrini, R.; Houdré, R.; Mulot, M.; Anand, S. & Smith, C. J. M. (2004). Temperature tuning of the optical properties of planar photonic crystal microcavities. *Applied Physics Letters*, Vol. 84, No. 6, 846-848

Wong, C.W.; Rakich, P.T.; Johnson, S.G.; Qi, M.; Smith, H.I.; Ippen, E.P.; Kimerling, L.C.; Jeon, Y.; Barbastathis, G. & Kim, S-G. (2004). Strain-tunable silicon photonic band gap microcavities in optical waveguides. *Applied Physics Letters,* Vol. 84, No. 8, 1242-1244

Yager, K.G. & Barrett, C.J. (2006). Novel photo-switching using azobenzene functional materials. *Journal of Photochemistry and Photobiology A: Chemistry*, Vol. 182, 250-26